JOURNAL OF SOLID STATE CHEMISTRY 41, 277–285 (1982)

# Neutron Diffraction Study of the Defect Pyrochlores $TaWO_{5.5}$, $HTaWO_6$, $H_2Ta_2O_6$, and $HTaWO_6 \cdot H_2O$

D. GROULT,* J. PANNETIER,† AND B. RAVEAU*

*Laboratoire de Cristallographie, Chimie et Physique des Solides, ISMRA, Université de Caen, 14032 Caen Cedex, France, and †Institut Laue Langevin, 156X, 38042 Grenoble Cedex, France

Received July 21, 1981; in final form October 21, 1981

The crystal structures of the defect pyrochlores $TaWO_{5.5}$, $HTaWO_6$, $DTaWO_6$, $H_2Ta_2O_6$, $D_{0.4}H_{1.6}Ta_2O_6$, and $HTaWO_6 \cdot H_2O$, have been investigated by neutron powder diffraction. By using conventional refinements, Fourier techniques, and electrostatic potential calculations the individual proton was found to be located in a partially occupied 48*f* position. At room temperature the oxygen of the water molecule resides in a 32*e* site close to the 8*b* position; the diffraction analysis at 4 K does not permit an unequivocal location of the water molecules but indicates a symmetry lowering induced presumably by the ordering of the water molecules.

## 1. Introduction

The possibility of cationic conductivity in the pyrochlore structure has been the subject of several studies (*1–3*). Although the search for fast-ion conductors with this structure has been somewhat disappointing, this class of materials remains attractive for model studies since the symmetry of the network is high (space group $Fd3m$) and many chemical substitutions are possible both on the skeleton and on mobile ion species.

The pyrochlore structure has described in many ways, but the defect $A_xM_2X_6$ pyrochlores may conveniently be represented as made up of an $[M_2X_6]$ skeleton of $(MX_6)$ corner-sharing octahedra with interstitial $A^+$ cations. If the $M$ cations are placed at the origin of the unit cell the $A^+$ cation ideally occupies either the 8*b* $(AM_2X_6)$ or the 16*d* $(A_2M_2X_6)$ sites. However, recent studies have provided evidence that this simple picture is not consistent with all observations. For instance, it has been shown that some $AM_2O_6$ pyrochlores depart from cubic symmetry (*1, 19*) and that the distribution of $A^+$ cations between 8*b* and 16*d* sites is rather complex for intermediate $A_{1+x}M_2X_6$ compositions (*3*). Furthermore, recent proton NMR measurements on $HTaWO_6$ and $HTaWO_6 \cdot H_2O$ (*6*) aimed at elucidating the nature of proton motion in these pyrochlores led to the conclusion that the water molecules randomly occupy one-half of the 16*d* sites (a result inconsistent with previous X-ray work (*5, 12*)), the individual protons being located in a 96*g* site close to a 16*d* position. We report here neutron powder diffraction results for $HTaWO_6$, its hydrate, and a series of related compounds; analysis of these results shows that the individual protons reside in a partially occupied 48*f* site as expected on electrostatic grounds.



0022-4596/82/030277-09$02.00/0

## 2. Experimental Methods

### 2.1. Materials Preparation

$HTaWO_6 \cdot H_2O$ was prepared from $KTaWO_6$ by ion exchange with aqueous 6 *M* $HNO_3$ following previously published methods (*4*). $HTaWO_6$ and $TaWO_{5.5}$ were obtained by dehydration of $HTaWO_6 \cdot H_2O$ at 300 and 530°C, respectively (*5*), and $DTaWO_6$ by reacting $HTaWO_6$ with $D_2O$ at 150°C, the hydration/dehydration cycles being performed four times. $H_2Ta_2O_6$ was obtained by dehydrating $H_2Ta_2O_6 \cdot H_2O$ at 250°C (*5*); deuteration was performed by heating $H_2Ta_2O_6$ under $D_2$ at 150°C.

The high incoherent scattering of hydrogen leads to a high background in the neutron powder patterns of protonated materials, that is, to a poorer peak to background ratio as compared to the deuterated analogs. However, preliminary neutron experiments on some of these pyrochlore compounds indicated that the $D^+ \rightleftarrows H^+$ exchange reaction was not always complete. As this work was aimed at finding the position of protons and water molecules in the channels of the pyrochlore structure we could not take the risk of studying incompletely exchanged samples and we decided to work with protonated materials. Reasonably good peak/background ratios were observed for all materials except $H_2Ta_2O_6 \cdot H_2O$, which was not studied further. Final refinements (see below) show that the $D^+ \rightleftarrows H^+$ exchange was complete for $HTaWO_6$ but not for $H_2Ta_2O_6$.

### 2.2. Neutron Diffraction

Powder neutron diffraction data were collected on the D1A high-resolution diffractometer (*7*) at the Institute Laue–Langevin with $\lambda = 1.3885(3)$ Å (nickel standard $a = 3.5238$ Å); a few restricted sets of data were also collected on the D1B position-sensitive detector diffractometer (*8*) with $\lambda = 1.2795(2)$ and 2.5246(2) Å. Samples of $TaWO_{5.5}$, $HTaWO_6$, and $DTaWO_6$ were sealed under vacuum in high-purity quartz ampoules; other samples were inserted in standard vanadium containers. For low-temperature experiments, the sample was held in a vanadium-tailed liquid helium cryostat. Data were collected from 10 to 160° in steps of 0.05° ($2\theta$), taking about 20 hr for each measurement. The raw data from the 10 counters were subsequently reduced by using conventional ILL programs (*9*). Integrated intensities and standard deviations were determined by fitting the shape of the Bragg peaks to Gaussian and the background to a first- or second-order polynomial (*9*). The cell parameters were obtained by least-squares refinement from the Bragg angles of the strongest lines, the zero-point correction of the instrument being included in the refinement. For all samples and temperatures the curves FWHM vs $\theta$ were consistent with the resolution function of the instrument; then, this most likely rules out any symmetry lowering at low temperature and all structural refinements were done in the cubic space group $Fd3m$. As the symmetry is high, there is almost no peak overlapping and we used a conventional integrated intensity refinement. The following scattering amplitudes (all $\times 10^{-12}$ cm) were used (*10*): −0.374(H), 0.667(D), 0.58(O), 0.70(Ta), and 0.48(W).

## 3. Structural Results

All refinements were done in space group $Fd3m$ (No. 227), the origin of the unit cell being taken at $\bar{3}m$ (origin $B_0$ according to (*11*)); Ta and W atoms are assumed to be statistically distributed over the 16*c* sites. The oxygen atoms of the network are located in 48*f* and their position is defined by a single parameter $x$(O).

### 3.1. $TaWO_{5.5}$

This is an unusual composition for a pyrochlore structure material and it can be

seen either as a regular pyrochlore framework containing extra cations in an interstitial position ($M_2O_6M'_{0.18}$) or as an oxygen-deficient framework $M_2O_{5.5}\square_{0.5}$. Although the former alternative would give an unlikely cation coordination we attempted a structure refinement with the interstitial metal atom in 16*d*, but the occupation number for this site converged to a slightly negative value. On the contrary, the latter hypothesis gives a stable solution with an occupancy factor of 0.97(4) for the oxygen position (48*f*) as compared to 0.917 calculated for $TaWO_{5.5}$. Therefore this composition should most likely be written as $TaWO_{5.5}\square_{0.5}$.

### 3.2. *$HTaWO_6$ and $DTaWO_6$*

A first refinement including only the framework atoms led to an $R$ factor ($R = \Sigma|I_0 - I_c|/\Sigma I_0$) close to 0.10. Using a Fourier difference technique the hydrogen atoms were then found to be localized in a partially occupied 48*f* site with $x \sim 0.4$. Further least-squares refinement of the scale factor, positional, and isotropic thermal parameters led to the results given in Table I.[1]

### 3.3. *$H_2Ta_2O_6$ and $D_2Ta_2O_6$*

The corresponding powder data were analyzed in a similar way and the hydrogen atoms were found to reside in the same partially occupied 48*f* site (Table I). However, refinement of the occupancy factor of this site from $D_2Ta_2O_6$ data showed the $D^+ \rightleftarrows H^+$ substitution to be incomplete, the calculated composition being $D_{0.4}H_{1.6}Ta_2O_6$.

### 3.4. *$H_3OTaWO_6$*

From previous X-ray work (*12*) it was concluded that the oxygen of the water molecule $O_W$ could be located either in the 8*b* site or in one of two possible 32*e* positions ($x$, $x$, $x$) in the vicinity of the 8*b* site ($x \sim 0.35$ or $x \sim 0.40$). From an analysis of their NMR data, Butler and Biefeld (*6*) suggested that the water molecules occupy randomly one-half of the 16*d* sites. All four solutions were then tested in least-squares refinement of the room-temperature data, the hydrogen atoms being excluded. Both the 8*b* and 16*d* solutions gave residuals of $R > 0.30$ and were therefore discarded; the two-32*e* hypothesis, involving only one more parameter, decreased the residuals to $R \sim 0.15$. The three hydrogen atoms were then localized on Fourier difference maps. One was found to reside in a 48*f* site identical to that of the proton in $HTaWO_6$ and the other two in a more general 96*g* site, close to $O_W$. The proton positional and thermal parameters were then refined and gave residuals of $R \sim 0.07$ for both possible positions of $O_W$ in 32*e*. A last Fourier difference map ($F$(exp) − $F(H_3TaWO_6)$) allows one to discard the $x \sim 0.40$ hypothesis. The final refined parameters are presented in Table II.

This structure solution was then applied to the 4-K data: the refinement quickly converged but the residuals remained rather high (Table II). The poorness of the fit definitely comes from the oxygen $O_W$ of the water molecule; both its positional and thermal parameters are strongly correlated (this was already observed for *RT* data) and $B(O_W)$ assumes an unreasonably high value. A possible delocalization of $O_W$ away from 32*e* sites was then probed: refinements involving the more general 96*g* sites led to atomic coordinates close to those of the 32*e* positions but $B(O_W)$ remained very large. A close examination of the 4-K powder pattern then revealed the existence of a few new lines (for instance, 550, 640, 642, 650, 653, 11.00, etc.) which can be indexed in the cubic cell but whose indexing is not compatible with an *F*-centered space group; the intensity of some of them rises up to 10% of the strongest reflections of the

[1] Lists of the observed and calculated intensities may be obtained through the laboratory.

TABLE I

FINAL REFINED PARAMETERS (NONHYDRATED PYROCHLORES)

| Compound | $T$ | λ (Å) | $a$ (Å) | $B(M)$ | $x$(O) | $B$(O) | $x$(H) | $B$(H) | NI[a] | $R^b$ (%) | $R_W{}^c$ (%) |
|---|---|---|---|---|---|---|---|---|---|---|---|
| $TaWO_{5.5}$[d] | *RT* | 1.3885(3) | 10.4372(6) | 2.42(16) | 0.3089(4)[e] | 1.01(6) | | | 46 | 8.22 | 7.77 |
| $HTaWO_6$ | 4 K | 1.3885(3) | 10.4438(5) | 1.74(15) | 0.3096(3) | 0.69(5) | 0.406(3)[f] | 2.2(8) | 37 | 6.38 | 6.28 |
| $HTaWO_6$ | *RT* | 1.3885(3) | 10.4443(6) | 2.03(15) | 0.3094(3) | 1.08(6) | 0.395(7)[f] | 6.2(18) | 44 | 6.42 | 6.31 |
| $DTaWO_6$ | *RT* | 1.3885(3) | 10.4425(6) | 2.51(19) | 0.3093(4) | 1.17(6) | 0.418(4)[f] | 6.0(9) | 46 | 8.13 | 8.31 |
| $D_{0.8}H_{0.2}TaWO_6$ | *RT* | 1.2795(2) | 10.4421(12) | 2.28(40) | 0.3108(7) | 1.13(12) | 0.400(9)[f] | 9.3(34) | 29 | 7.45 | 4.95 |
| $H_2Ta_2O_6$ | *RT* | 1.3885(3) | 10.6032(6) | 1.82(16) | 0.3109(5) | 1.06(8) | 0.402(4)[g] | 5.4(10) | 42 | 8.72 | 8.11 |
| $D_{0.4}H_{1.6}Ta_2O_6$ | *RT* | 1.3885(3) | 10.6106(6) | 1.88(15) | 0.3107(5) | 1.22(9) | 0.391(8)[g] | 3.4(26) | 42 | 8.51 | 7.34 |

*Note.* ESD are given in parentheses and refer to the last digit.

[a] NI = number of intensities used in the refinement.

[b] $R = \Sigma|I_0 - I_c|/\Sigma I_0$.

[c] $R_W = [\Sigma_W|I_0 - I_c|^2/\Sigma_W I_0^2]^{1/2}$.

[d] For all Ta/W compounds, the metal atoms are assumed to be statistically distributed over 16*c* sites.

[e] Occupancy factor 5.5/6.

[f] Occupancy factor $\frac{1}{8}$.

[g] Occupancy factor $\frac{1}{3}$.

TABLE II

FINAL REFINED PARAMETERS ($H_3OTaWO_6$)

| Temperature | | *RT* | 4 K[a] |
|---|---|---|---|
| $a$(Å) | | 10.3999(5) | 10.3927(10) |
| $B(M)$ | 16*c*[b] | 1.37(13) | 1.62(22) |
| $x$(O) | 48*f* | 0.3104(4) | 0.3098(5) |
| $B$(O) | 48*f* | 0.92(6) | 0.84(8) |
| $x$(H) | 48*f* | 0.415(5) | 0.413(15) |
| $B$(H) | 48*f* | 3.3(9) | 7.7(34) |
| $x(O_w)$ | 32*e* | 0.355(3) | 0.347(9)[a] |
| $B(O_w)$ | 32*e* | 8.9(14) | 11.5(64)[a] |
| $x(H_w)$ | 96*g* | 0.355(3) | 0.352(3) |
| $z(H_w)$ | 96*g* | 0.282(5) | 0.269(5) |
| $B(H_w)$ | 96*g* | 4.7(12) | 2.3(11) |
| $R$(%) | | 6.4 | 10.3 |
| $R_w$(%) | | 6.5 | 9.3 |

[a] These results correspond to the best refinement in space group $Fd3m$; however, the true symmetry at 4 K is lower (cubic $P$ space group), from which arise the anomalous values of the $O_w$ parameters (see text).

[b] Ta/W statistically disordered.

pattern. None of these lines is observed on $HTaWO_6$ (4 K) or on $HTaWO_6 \cdot H_2O$ (*RT*) data. Then this is clear evidence of a change of space group at low temperature; as no line broadening is observed, one can assume that the cubic symmetry is preserved.

## 4. Discussion

### *4.1. $TaWO_{5.5}$*

This is the first structural characterization of a cubic pyrochlore with an oxygen-deficient network, although nonstoichiometry has already been observed in related structures (*13*). The way the framework can accommodate the oxygen vacancies is not yet understood but it is worth noting that the transformation $HTaWO_6 \rightarrow TaWO_{5.5}$ leads only to a small decrease of the cell volume (0.06%) and that this is most likely the maximum amount of vacancies the lattice can tolerate; indeed the dehydration of $H_2Ta_2O_6$ leads directly to $\delta$–$Ta_2O_5$ without any intermediate pyrochlore phase (*5*). $TaWO_{5.5}$ is hygroscopic and rehydrates to $TaWO_{5.5} \cdot 0.75\ H_2O$ (*5*). However, this hydrate loses water above room temperature (*12*), which means the water molecules are only weakly bound to the solid; then they must be located in the channels of the $TaWO_{5.5}$ network and must not replace the vacancies on the main oxygen lattice (this is also in agreement with the decrease of cell volume observed during the hydration of $TaWO_{5.5}$ (*5*)).

### *4.2. $HTaWO_6$ and $H_2Ta_2O_6$*

Neutron diffraction data definitely rule out the localization of $H^+$ in the vicinity of the 16*d* sites as suggested by Butler and Biefeld (*6*) and Rotella *et al.* (*14*) for $HTaWO_6$. This is further demonstrated by calculating the potential energy map of the pyrochlore channels. Indeed one possible approach for determining the position of hydrogen or, more generally, of light atoms in inorganic structures is to minimize the total lattice energy with respect to the proton (or light atom) coordinates (*15–17*); this is conveniently done by minimizing the electrostatic part of the lattice energy while constraining the oxygen–proton (or oxygen–light atom) distance to some reasonable value. However, such a straightforward approach is difficult to use for the pyrochlore structure because of the high symmetry of the cage centered on the 8*b* position, from which results a partial occupancy of the proton sites; such a random distribution of charges over equivalent positions then leads to some difficulties in calculating the lattice sums (*18*). In view of that difficulty we moved to a simpler semi-quantitative approach: all calculations were done for a hypothetical $M_2^{6+}O_6^{2-}$ pyrochlore structure; clearly the results do not allow one to evaluate the potential barrier (i.e., the activation energy (*19*)) of the proton motion, but we believe they provide a

rather realistic picture of the potential profile in the cavities of the pyrochlore structure.

The electrostatic potential was evaluated by the Bertaut method (*20, 21*) using a linear charge distribution and a series termination at $\beta = 3\pi$. Calculations were restricted to a part of the (110) plane centered on the 8*b* position ($x, y, z = \frac{3}{8}, \frac{3}{8}, \frac{3}{8}$); the potential was calculated at the grid points of a regular rectangular mesh; the step between the grid points was 0.025 (reduced coordinates), which corresponds to 0.26 Å with a cell parameter of 10.45 Å.

The resulting map is shown in Fig. 1. The first striking feature of this map is the flatness of the potential in the vicinity of the 8*b* center; indeed this is in agreement with the large values of the isotropic Debye–Waller parameters usually obtained for the *A* cation in the $A^+M_2X_6$ pyrochlores (*22*). More important is the fact that the 8*b* site is not a true minimum of the potential but only a plateau in the potential map (the

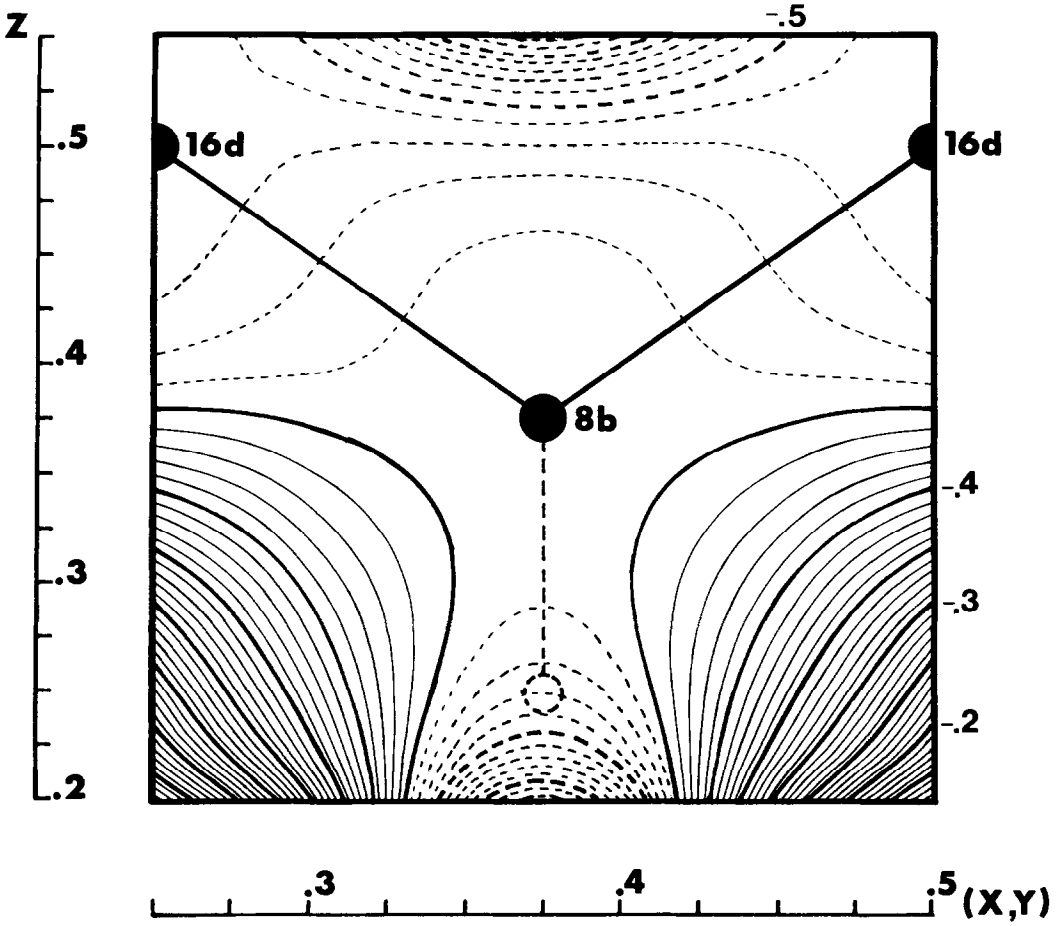


FIG. 1. Electrostatic potential map: potential in atomic units ($eÅ^{-1}$) for a hypothetical pyrochlore $M_2^{\frac{8}{3}+}O_6^{2-}$ with $a = 10.45$ Å. The difference between adjacent lines ins 0.01 $eÅ^{-1}$. The dashed circle is the projection of two 16*d* nearest-neighbor sites on the plane of the map (110). The full and dashed equipotential lines correspond, respectively, to potential values higher and lower than the 8*b* potential.

electrostatic field goes to zero at the point $\frac{3}{8}$, $\frac{3}{8}$, $\frac{3}{8}$). The 16*d* position is a local minimum of the potential (at 0.03 eÅ$^{-1}$ below the 8*b* potential), but the deepest potential well is found along the (001) direction (or along the equivalent (100) and (010) directions), i.e., by moving from 8*b* toward the anion located at $\frac{3}{8}$, $\frac{3}{8}$, $1 - x$(48*f*) or $\frac{3}{8}$, $\frac{3}{8}$, $x$(48*f*) $- \frac{1}{4}$. It is worth mentioning, however, that, whereas the 16*d* site is a true minimum of the *electrostatic* potential, there is no such local minimum along (001) but only a steep decrease of the potential: then it is the addition of the overlap repulsion energy which will eventually yield a minimum of the *total crystal energy* along this direction. As a consequence, the 8*b* position is always unstable (*23*) within the $(M_2X_6)^-$ framework, but the displacement of an $A^+$ cation from 8*b* along either one of the four (111) or one of the six (001) equivalent directions will depend critically on the balance between electrostatic and short-range forces; therefore no general rule can be given for the location of large $A^+$ cations. However, the small size of the proton makes it a well-adapted probe to study the potential profiles in the pyrochlore cavities: with the constraint that the O–H distance does not become shorter than about 1 Å, the proton will sit in the deeper electrostatic potential well. The potential map (Fig. 1) then clearly shows that the proton must be displaced from 8*b* to one of the 48*f* positions associated with each 8*b* position, in agreement with the analysis of the neutron data.

It is worth mentioning too that the second moment calculated for a random distribution of protons over the 48*f* sites ($M_2$ = 1.35 G²) is in fair agreement with the measured second moment obtained by numerical integration for $HTaWO_6$: $M_2$(exp) = 1.3 G² (*6*).

From a structural point of view, it should be noted that the values of $x$(O) for $HTaWO_6$ are unusually small; they are indeed less than the ideal value $x = 0.3125$ which corresponds to a metrically undistorted ($MO_6$) octahedron. As a consequence, the ($MO_6$) octahedron in $HTaWO_6$ and $H_2Ta_2O_6$ are slightly elongated along a threefold axis; the explanation is to be found in the average coordination number of the oxygen atoms, which is less than that in the nonprotonated $AM_2O_6$ ($CN$ = 3) or $A_2M_2O_6$ ($CN$ = 4) pyrochlores.

### 4.3. $HTaWO_6 \cdot H_2O$

Although the 4-K results unambiguously indicate a change of space group we feel the room-temperature data are consistent with a $Fd3m$ model. Both the $(TaWO_6)^-$ skeleton and the individual proton occupy the same position as in $HTaWO_6$ (Table III), which means that the structure is not affected by the hydration process, i.e., that the interaction between the water molecule and $HTaWO_6$ is rather weak (the water molecule is lost, reversibly, above 100°C). In agreement with proton NMR results (*6*) there is no $H_3O^+$ species in the structure; however, the oxygen of the water molecules resides in the vicinity of the 8*b* site and not in a 16*d* position. The proton $H_W$ of the water molecules is 0.97(5) Å from the oxygen atom and 1.67(6) Å from the other proton, which is a common geometry for water molecules in crystalline hydrates (*15, 24*). The orientation of the water molecule is obviously determined by the electrostatic interaction between the $H_2O$ molecule and the $HTaWO_6$ network, the protons

TABLE III

INTERATOMIC DISTANCES (Å)

| Compound | $T$ | $M$–O | O–H |
|---|---|---|---|
| $TaWO_{5.5}$ | *RT* | 1.945(1) | — |
| $HTaWO_6$ | 4 K | 1.948(1) | 1.01(3) |
| $HTaWO_6$ | *RT* | 1.948(1) | 0.90(7) |
| $DTaWO_6$ | *RT* | 1.947(1) | 1.13(4) |
| $HTaWO_6$, $H_2O$ | 4 K | 1.939(1) | 1.07(15) |
| $HTaWO_6$, $H_2O$ | *RT* | 1.943(1) | 1.09(5) |
| $H_2Ta_2O_6$ | *RT* | 1.982(2) | 0.97(4) |

$H_W$ pointing toward the positions of minimum potential (48*f*), while the oxygen atom is located close to the 8*b* potential plateau. This oxygen $O_W$ is 2.00(6) Å from the individual proton, but the shortest distance from the proton $H_W$ to the framework oxygen is 2.32(5) Å, which corresponds to a weak hydrogen bond. The resulting H---$OH_2$ configuration (Fig. 2) is an almost planar isosceles triangle, in a manner intermediate between a true $H_3O^+$ ion and two separate $H^+$ and $H_2O$ species.

The thermal parameters of the water molecule are fairly high but they compare well to the values obtained for zeolite materials (for instance, $B(H_W) = 10$ and $B(O_W) = 7$ Å$^2$ in analcite (*25*)); tumbling of the water molecule was indeed observed above 300 K by NMR (*6*). By considering a single isolated cage centered on an 8*b* site (Fig. 2) and assuming that the isolated proton is fixed in one of the six possible 48*f* sites, one can see that there are two equivalent positions for the water molecules (they are related by a mirror plane); the motion observed above 200 K is presumably due to the jump between these two positions; translational motion begins above room temperature and leads to a loss of water.

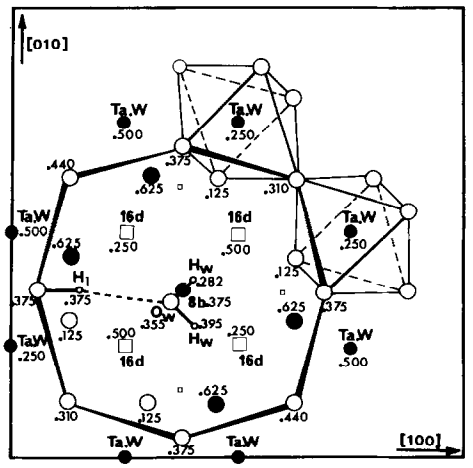


FIG. 2. Water molecule coordination inside a cage of the pyrochlore structure. The large open circles represent oxygens.

At 4 K the motion of the water molecule, as seen by NMR, is frozen and the diffraction results suggest that the $HTaWO_6$ network is not noticeably modified (Table II); this is also consistent with the "normal" behavior of $HTaWO_6$ at low temperature (no symmetry lowering). The change of symmetry of $HTaWO_6 \cdot H_2O$ at low temperature (from a cubic *F* to, at the most, a *P* cubic space group) is then a strong indication of an ordering of the water molecules inside the channels of the pyrochlore structure. Although the scarcity of data from powder diffraction does not allow one to determine unambiguously the low-temperature space group and then the ordered structure of the water molecules, one may reasonably explain the 4-K results by the following model: below a critical temperature (presumably about 200 K) the water molecule is frozen in one of the two equivalent positions quoted above; there is, however, enough electrostatic interaction between two neighbor cages to prevent random freezing. This ordered arrangement can be either a consequence of an ordering of the individual protons in the structure or a result from a direct interaction between the water molecules; the fact that $HTaWO_6$ does not show any apparent ordering at low temperature supports the latter hypothesis. It is worth mentioning that this ordering phenomenon is doubtlessly influenced by the local arrangements of the Ta and W atoms on the 16*c* sites; $H_2Ta_2O_6 \cdot H_2O$, which does not have this problem of disorder on the cationic positions, would then be a better candidate for studying the ordered structure of the proton and water molecules in the pyrochlore structure.

## Acknowledgment

The authors would like to thank J. Lamotte (Laboratoire de Spectroscopie Moléculaire, ISMRA, Caen) for

his technical assistance in the preparation of the deuterated compounds.

## References


1. A. W. SLEIGHT, J. F. GULLEY, AND T. BERZINS, *ACS Advan. Chem. Ser.* **163,** 95 (1977).
2. J. B. GOODENOUGH, H. Y.-P. HONG, AND J. A. KAFALAS, *Mater. Res. Bull.* **11,** 203 (1976).
3. A. D. ENGLISH, A. W. SLEIGHT, J. L. FOURQUET, AND R. DE PAPE, *Mater. Res. Bull.* **15,** 1727 (1980).
4. M. HERVIEU, C. MICHEL, AND B. RAVEAU, *Bull Soc. Chim. Fr.* **11,** 3939 (1971).
5. C. MICHEL, D. GROULT, AND B. RAVEAU, *J. Inorg. Nucl. Chem.* **36,** 61 (1974).
6. M. A. BUTLER AND R. M. BIEFELD, *Phys. Rev. B* **19,** 5455 (1979).
7. A. W. HEWAT AND I. BAILEY, *Nucl. Instrum. Methods* **137,** 463 (1976).
8. R. ALLEMAND, J. BOURDEL, E. ROUDAUT, P. CONVERT, K. IBEL, J. JACOBÉ, J. P. COTTON, AND B. FARNOUX, *Nucl. Instrum. Methods,* **126,** 29 (1975).
9. P. WOLFERS, "Programs for Treatment of Powder Profiles," private communication (1975).
10. G. E. BACON, "The Neutron Diffraction Newsletter" (W. B. Yelon, Ed.).
11. A. W. SLEIGHT, *Inorg. Chem.* **7,** 1704 (1968).
12. C. MICHEL, Thèse de doctorat es-sciences, Caen (1974).
13. M. GOREAUD, G. DESGARDIN, AND B. RAVEAU, *J. Solid State Chem.* **27,** 145 (1979).
14. F. J. ROTELLA, J. D. JORGENSEN, B. MOROSIN, AND R. M. BIEFELD, *Bull. Amer. Phys. Soc.* **26,** 371, HB+4 (1981). These authors reported on neutron diffraction of $DTaWO_6$ and arrived at the same conclusion.
15. W. H. BAUR, *Acta Crystallogr.* **19,** 909 (1965).
16. R. F. GIESE, *Science* **172,** 263 (1971).
17. R. F. GIESE, *Acta Crystallogr. B* **32,** 1719 (1976).
18. W. W. BARKER, P. S. WHITE, AND O. KNOP, *Canad. J. Chem.* **54,** 2316 (1976).
19. J. PANNETIER, *Solid State Commun.* **34,** 405 (1980).
20. E. F. BERTAUT, *J. Phys. Chem. Solids* **39,** 97 (1978).
21. E. F. BERTAUT, *J. Phys.* **39,** 1331 (1978).
22. D. BABEL, *Z. Anorg. Allg. Chem.* **387,** 161 (1972).
23. J. PANNETIER, *J. Phys. Chem. Solids* **34,** 583 (1973).
24. G. FERRARIS AND M. FRANCHINI-ANGELA, *Acta Crystallogr. B* **28,** 3572 (1972).
25. G. FERRARIS, D. W. JONES, AND J. YERKESS, *Z. Kristallogr. Bd.* **135,** 240 (1972).